CHEMISTRY
A EUROPEAN JOURNAL

Supporting Information

Efficient Charge Injection from the S_2 Photoexcited State of Special-Pair Mimic Porphyrin Assemblies Anchored on a Titanium-Modified ITO Anode

Mitsuhiko Morisue, Dr.[†], Noriko Haruta, Dipak Kalita, Dr.,

and Yoshiaki Kobuke, Prof.*

Graduate School of Materials Science, Nara Institute of Science and Technology

8916-5 Takayama, Ikoma, Nara 630-0192 (Japan)

FAX: (+81)743-72-6119

E-mail: kobuke@ms.naist.jp

[†]Present Address: *Department of Biomolecular Engineering*

Kyoto Institute of Technology, Matsugasaki, Sakyo-ku, Kyoto 606-8585 (Japan)

1. Blocking Experiments: If the surface-confined species covers the whole ITO surface, the redox process between the electrode and bulk electrophore should be insulated. The titanium layer was investigated by using $K_3Fe(CN)_6$ as a bulk redox probe. No substantial change of the redox couple of bulk $K_3Fe(CN)_6$ was found in CVs by using titanium modified ITO working electrodes compared with bare ITO electrode (Figure S1). It means that the titanium layer does not insulate the redox process between ITO electrode and the outer redox site.

In the same manner, an SP-mimic porphyrin dimer was characterized. Retardation of the redox process of $K_3Fe(CN)_6$ suggests that the porphyrin insulating layer possesses many pin-hole sites to allow the $K_3Fe(CN)_6$ redox site access the electrode surface.

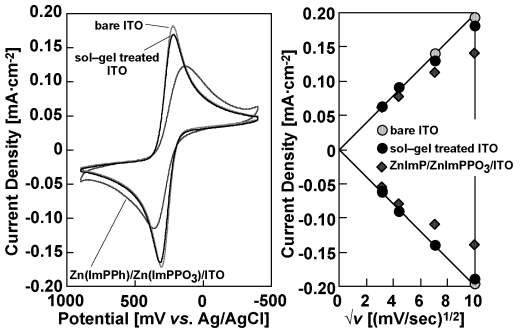

Figure S1. Cyclic voltammograms of 1.0 mM $K_3Fe(CN)_6$ in buffered aqueous solution (pH 6.2) by using bare ITO, titanium-treated ITO, and SP-mimic immobilized ITO working electrodes at 100 $mV \cdot sec^{-1}$ of scan rate (left) and the plot of the corresponding peak current as a function of square root of scan rate (right).

2. XPS spectra: Survey XPS spectra were shown in Figure S2. Magnified spectra and their deconvoluted profiles for C(1s), N(1s), Sn(3d), and Zn(2p) region were shown in Figure 5. The spectra shown in Figures S2 and S3 were obtained at a take-off angle of 60°, illustrating almost the same spectral shape at a take-off angle of 15° (data not shown), except for O(1s) as shown in text (Figure 3). This comparison claims that the porphyrin layers are considerably thin.

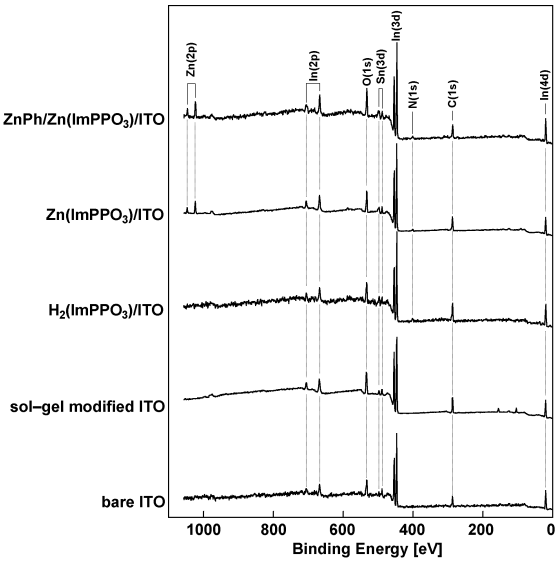

Figure S2. Survey XPS spectral change of ITO surface in the course of an SP-mimic dimer formation: bare ITO, sol–gel modified ITO, H_2(ImPPO$_3$)-assembled ITO, Zn(ImPPO$_3$)/ITO, and Zn(ImPPh)/Zn(ImPPO$_3$)/ITO (lower to upper). Spectra were observed at a take-off angle of 60° by using monochromatic Al K_α (1486.6 eV).

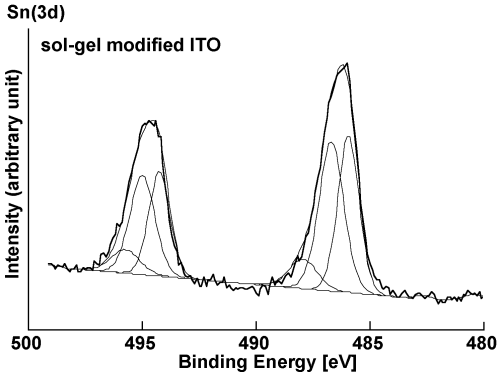

Figure S3. XPS deconvoluted profile of sol-gel modified ITO surface in Sn(3d) region observed at a take-off angle of 60° by using monochromatic Al K_α (1486.6 eV).

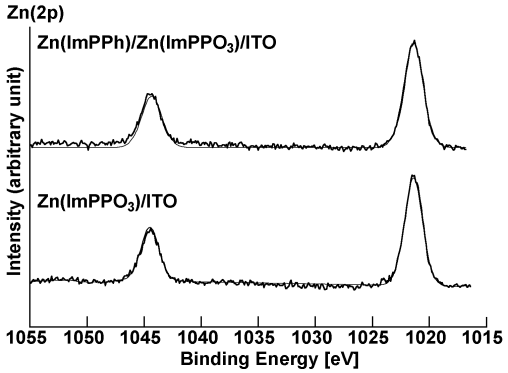

Figure S4. XPS deconvoluted profiles of $Zn(ImPPO_3)$/ITO and $Zn(ImPPh)/Zn(ImPPO_3)$/ITO surface in Zn(2p) region observed at a take-off angle of 60°.

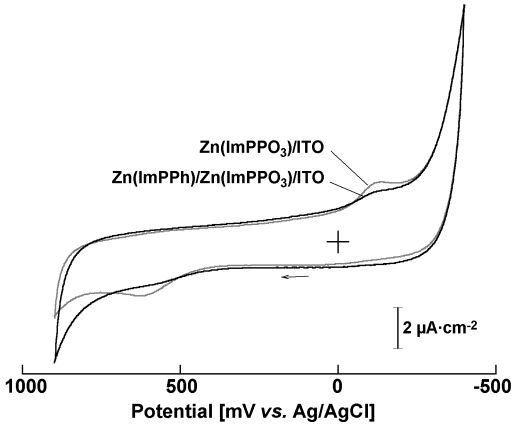

Figure S5. Cyclic voltammograms of $Zn(ImPPO_3)$/ITO and $Zn(ImPPh)/Zn(ImPPO_3)$/ITO in aqueous solution with 1.0 M $NaClO_4$ electrolyte under nitrogen stream at 50 $mV \cdot sec^{-1}$.

3. Cyclic Voltammetry: Characterization of the immobilized porphyrins, $Zn(ImPPO_3)$/ITO and $Zn(ImPPh)/Zn(ImPPO_3)$/ITO, was attempted by means of cyclic voltammetry (CV) (Figure S5). SP-mimic dimer formation decreased the electrochemical response, probably due to increasing hydrophobicity and less permeability of electrolyte. CV measurements observed no substantial difference of the redox potential depending on the anchoring species, except the magnitude of peak current. Zn porphyrin was oxidized around 610 mV, which was almost identical to that observed generally in organic solvent. This oxidation potential showed no sweep rate dependence, indicative of the surface-bound redox process. The generated cation was reversibly reduced around –100 mV. Potential sweep cycles over 0 mV lost the oxidation wave around 610 mV in the second potential sweep. On the other hand, the oxidation wave was reversibly observed during potential sweep over –400 mV (Figure 6). The reduction wave around –100 mV is therefore assignable to the reduction wave of the porphyrin cation.

Extremely large peak potential separation ($?E = E_{ox} - E_{red}$) is probably ascribable to significant stabilization of the generated cation radical by the reorganized environmental water molecules. According to the Butler–Volmer kinetic theory, that is general formalism for electrode reaction, assumes that the free energy of the electron transfer barrier is much smaller than reorganization energy.[52] Thus, electron transfer between an electrode and redox sites is desired to show zero peak potential separation for diffusion-less processes in the ideal principle. The $?E$ for the porphyrin dimer, however, reaches to 720 mV. Such observation implies that the present redox process is irreversible in an electrochemical sense. Based on the Marcus theory of electron transfer, the reorganization energy of the environmental solvent molecule increases as its polarity becomes higher in the "normal" regime.[53] In the "inverted" region, on the other hand, the backward process requires very high driving force, even though the forward electron transfer reaction proceeds smoothly. Previous spectroscopic observation on the photoinduced charge-separation has suggested that forward electron transfer reaction of the SP-mimic

porphyrin dimer occurs in the "normal" region, while the backward process proceeds in the "inverted" regime of the Marcus parabola.[21] The electrochemical process is in principle different from the photoinduced electron transfer reaction. The irreversibility of the redox process may suggest large stabilization by solvent molecule or electrolyte as well as very slow electron transfer kinetics.[40c] The generated cation may be stabilized by reorganizing water molecules, although the forward redox process of the SP-mimic porphyrin dimer in aqueous environment can proceed smoothly. Therefore regeneration of hydrophobic neutral porphyrin will be unfavorable in aqueous media. The oxidized SP-mimc dimer can remain the cation radical with appropriate persistence in aqueous media on the electrode surface.

4. Anodic photocurrent generation: The dark current is ascribable to oxidation of bulk hydroquinone, therefore depends on the pH conditions. On acidifying the pH, the oxidation potential of hydroquinone shifted to more anodic and therefore the dark current decreased even at higher bias potentials. Even though the quantum yield for anodic photocurrent gives significantly different values at each potential, the dark current for each electrode ranged in similar levels as shown in Figure S5.

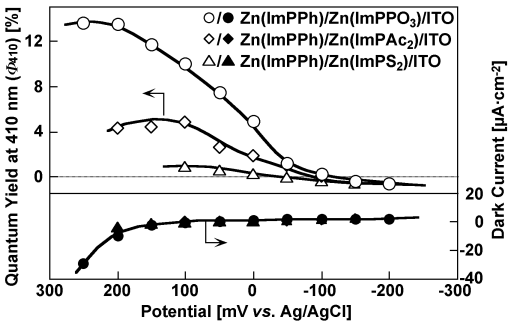

Figure S6. Potential dependence of quantum yield at 410 nm and dark current for Zn(ImPPh)/Zn(ImPPO$_3$)/ITO, Zn(ImPPh)/Zn(ImPAc$_2$)/ITO, and Zn(ImPPh)/Zn(ImPS$_2$)/ITO in the presence of 50 mM hydroquinone with 1.0 M $NaClO_4$ supporting electrolyte (pH 6.2) at 100 mV *vs.* Ag/AgCl.

Appendix

The IPCE (incident photon–to–current conversion efficiency) value is determined as follows:

$$\text{IPCE (\%)} = 100\,(i/e)/(W\,l/hc)$$

wherein i, W, and l are anodic photocurrent density [A cm^{-2}], the incident photon flux, and wavelength [nm], respectively. IPCE is an index to evaluate the total profile of the photosensitizing cell at each wavelength. To evaluate the efficiency for conversion of the absorbed photon to current, photocurrent quantum yield F was employed. The quantum yield F is defined as the following equation:

$$F = \text{IPCE/LHE}$$

wherein LHE is light harvesting efficiency (LHE = $1–10^{-A}$).

References

[21] H. Ozeki, A. Nomoto, K. Ogawa, Y. Kobuke, M. Murakami, K. Hosoda, M. Ohtani, S. Nakashima, H. Miyasaka, T. Okada, *Chem. Eur. J*. **2004**, *10*, 6393.

[40] c) H.-G. Hong, W. Park, *Langmuir* **2001**, *17*, 2485.

[52] A. J. Bard, L. R. Faulker, *Electrochemical Methods, Fundamentals and Applications* (John Wiley & Sons) **1980**.

[53] R. A. Marcus, N. Sutin, *Biochim. Biophys. Acta* **1985**, *811*, 265.